Sustainable Hydrogen Production via LiH Hydrolysis for Unmanned Air Vehicle (UAV) Applications

Martin Khzouz[1], Evangelos I. Gkanas[1*], Alessandro Girella[3], Thomas Statheros[2], Chiara Milanese[3]

[1]*Hydrogen for Mobility Lab, Institute for Future Transport and Cities, Coventry University, Cheetah Road, Chamber House IV09, CV1 2TL, Coventry, UK*

[2] *School of Mechanical, Automotive and Aersopace Engineering, Coventry University, Priory Street, CV1 5FB, Coventry, UK*

[3]*Pavia Hydrogen Lab, C.S.G.I. & Dipartimento di Chimica, Sezione di Chimica Fisica, Università di Pavia, Viale Taramelli 16, 27100 Pavia, Italy*

[*]*Correspondent author: ac1029@coventry.ac.uk*

Abstract:

In the current study, an experimental approach for the further understanding of the LiH hydrolysis reaction for hydrogen production is considered. The experimental work has been undertaken under small scale conditions by utilising fixed bed reactors. The hydrolysis reaction has been studied at several oven temperatures (150 ^{o}C, 300 ^{o}C and 500 ^{o}C). The favourable driving potentials for the hydrolysis reactions were identified by the utilization of the Gibbs free energy analysis. The main outcome of the study is the deceleration of the reaction pace due to the formation of the by-product layers during the reaction. At the initial stage, due to the contact of steam with the unreacted and fresh LiH surface, the reaction proceeds on a fast pace, while the formation of the layers tends to decelerate the diffusion of steam into the core of material, forcing the production step to be slower. The hydrogen yield was found to be more than 90% of the theoretical value for all the reaction temperatures. Finally, a scenario of a hybrid-electric propulsion system for Unmanned Aerial Vehicles (UAVs) including Li-ion battery, Proton Membrane Fuel Cell (PEMFC) and an on-board hydrogen production system based on LiH hydrolysis is introduced and studied.

Keywords:
Hydrogen Production; Metal hydrides, LiH hydrolysis; Steam hydrolysis, Hydrogen generator, Unmanned Aerial Vehicles

Highlights:

- *A hydrogen production yield of 90% via steam LiH hydrolysis was achieved*
- *The reaction rate was found to be intense and aggressive at the first phase of the reaction*
- *The reaction rate was found to decelerate due to the formation of by-products*
- *Maintaining the exothermic reaction is essential for high yield hydrogen production*

1. Introduction

The increasing of the global population in combination with the need to increase the human living standards has led to a high global energy demand [1, 2]. Currently, almost 85% of the total global energy consumption is obtained from non-renewable resources such as coal, oil and natural gas [3]. The usage of such resources contributes negatively to environmental issues (air pollution, greenhouse gas emissions and global warming) as well as to political, financial and humanitarian crises [4 - 7]. These resources are finite, and the reserves are depleting which results in economic and political uncertainties. Thus, it is essential to develop a reliable, affordable and sustainable energy system based on renewable energy agents [8, 9]. Over the last decades, the investigation for sustainable alternative fuels and energy technologies to replace fossil fuel technologies has been out of significant importance for the future energy stability [10-13]. Hydrogen appears to be a potential energy solution for a carbon free society and economy [14-16]. For the establishment of a global hydrogen-based economy, hydrogen has to be treated as any other product. It has to be produced, stored, transported, delivered and used [17]. Hydrogen is an abundant element and the most available renewable energy carrier [18]; it is also deemed to be the suitable solution to the environmental problems, if produced from renewable resources [19, 20]. Indeed, it can be produced from many sources, both renewable and non-renewable, such as water (via electrolysis) [21], hydrocarbon fuels [22], biomass [23], water splitting by solar energy and the hydrolysis of hydrides and/or chemical elements that include hydrogen [24]. Different hydrides such as the metal hydrides [25, 26] as LiH [27], the borohydrides as $NaBH_4$ [28], $LiBH_4$ [29], and Ammonia Borane [30] have been reported as potential sources for effective hydrogen production. Each one of the aforementioned cases, require a different process of chemical treatment and each hydrolysis reaction is more efficient at different temperatures. The selection of each hydride for fast hydrogen production, besides the criterion for large

hydrogen storage capacity, depends on the reaction limitations and the formation of the reaction products.

Hydrogen is also a very common fuel source for fuel cells. Fuel cells are electrochemical cells that are able to utilise the fuel under nearly thermodynamically reversible condition as compared to the simple combustion engines [31]. Unmanned Aerial Vehicles (UAVs) have been received special attention due to their potential applications in several sectors, such as surveillance and firefighting [32]. The most common propulsion system for UAVs is the utilisation of batteries (electric propulsion systems) [33]. The main drawback of this technology lies upon the limited flying range that can be achieved [34]. A possible solution to that issue might be the usage of fuel cells for electricity generation [35]. In that case, the only limitation is the amount of fuel (hydrogen) that the UAV can carry [36]. The most common way to store hydrogen for mobility applications is at high pressure when utilising high pressure storage tanks. One of the challenges besides hydrogen storage is the on-demand and real-time hydrogen production to be used from fuel cells, especially for emergency situations (backup power unit sources). The produced hydrogen will be able to provide enough fuel to the cells to operate and land the UAV for longer endurance time.

Lithium hydride (LiH) is an attractive material that can be used in the field of new energy technologies such as controlled fusion, fuel cells and neutron shielding [37]. LiH presents large hydrogen storage capacity (12 wt%) [38], and its high reactivity with water makes it a very attractive candidate to be utilised as hydrogen generator [39]. However, the kinetics of the hydrolysis reaction must be identified, measured and enhanced in order LiH to become an effective hydrogen generator for low power demand applications, such as fuel cells [40]. LiH is a material whose implementation requires a strict control of storage and handling. The reaction of LiH with water is highly exothermic and the control of the temperature increase during the reaction itself is of major importance [41]. Thus, LiH must be handled and

protected under inert atmosphere to prevent any risk of unnecessary reaction with the atmospheric humidity and inflammation [42]. A limited number of studies have been conducted in order to extract information regarding the kinetics of the reaction and the behaviour of LiH in the presence of water [43-45]. A common denominator of these studies is that during the hydrolysis reaction, a dual LiH/Li_2O/LiOH interface is formed. Li_2O is assumed to play the role of a protective layer which will affect the further diffusion of H_2O to LiH [46]. Some reports do not mention or take into account the Li_2O layer, as it is very difficult to be detected. A thin layer (~100-120 Å) is expected to form at room temperature [37]. Besides the contradictory conclusions regarding the reaction schemes and the species involved within those studies, it is commonly accepted that regarding the hydrolysis of LiH, the reaction kinetics are strongly influenced by the temperature, the water vapor pressure, the amount of the LiH material and the LiH powder packing conditions [47].

In the current work, the hydrolysis reaction of LiH at several reaction temperatures is examined, when introducing water steam within the reactor. The objectives of the study are the investigation and understanding of the reaction at that temperature range, to investigate the hydrogen production rate, the hydrogen production yield and the composition of the products after the reaction, for possible usage of the produced hydrogen for Fuel Cell/Electric Hybrid Fuel Cell UAVs. The hydrolysis reaction was investigated at oven temperatures of 150 ^{o}C, 300 ^{o}C and 500 ^{o}C and the hydrogen production capacities were recorded as well as the temperature distribution during the hydrolysis reaction. The identification of the by-products of the reaction is very important, as the formation of the by-product layers can affect the reaction rate. X-ray diffraction analysis was used to identify the by-products and also the feasibility of the possible reactions was studied by the investigation of the Gibbs free energy and the chemical equilibrium analysis. The hydrolysis of lithium hydride using water steam showed that the by-product formation did not affect the amount of hydrogen produced but the

reaction rate and the duration of the reaction were affected by the presence of the by-products.

2. Experimental Procedure

2.1 Materials and Sample Preparation

The preparation of the material was conducted under dry atmosphere. All the LiH samples were extracted from the same powder batch in order to ensure the homogeneity of the results. Fine powder of LiH was utilized (30 mesh size, 95% purity, Sigma Aldrich). The preparation of all the samples was performed under dry atmosphere (Ar) using an MBraun LABstar glove box to avoid any contact with the atmospheric moisture and the atmospheric contamination (H_2O, O_2, CO_2…). Distilled water (H_2O) was employed for the hydrolysis reaction.

2.2 Experimental Setup and Equipment

The experimental setup utilised for the hydrolysis reaction is shown in Fig. 1. The fixed bed reactor was made in stainless steel 316L (Swagelok) with internal diameter of 10.9 mm. The outlet of the reactor bed was packed with quartz wool to prevent the small particles of the powder to pass into the ¼" pipe system. Once the packed reactor was filled with LiH powder (approximately *one gram*) in each trial, the reactor was connected to the rest of the apparatus under continuous Ar flow to avoid oxidation and contamination of the system. The flow rate for Ar was 10 ml/min and it was kept for additional 20 minutes to ensure that the whole piping system was purified and minimised the oxygen traces within the pipe. Then, Ar was switched off and the flow of gas inside the entire piping system was left to pass through the outlet pipes for an extra 30 minutes. The hydrolysis reaction was initiated when a controlled amount of water (0.3 ml/min) was injected by using a syringe pump (Cole Parmer) equipped with a 10 ml volume syringe.

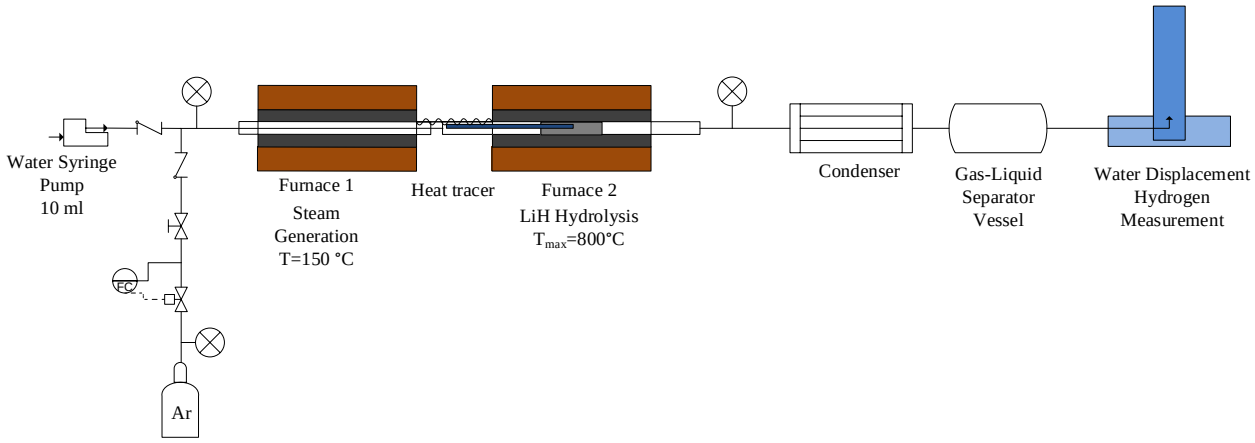

Fig. 1. Experimental apparatus developed and used for the LiH hydrolysis reaction and the measurement of the produced hydrogen.

As shown in Fig. 1, the water was injected into the first furnace (Furnace 1), where the temperature of the oven was kept constant at 150 ^{o}C and water steam was produced. Then, a second furnace (Furnace 2) was utilised to control the temperature of the hydrolysis reaction using a PID controller (Omega). A K-type thermocouple was introduced in the reactor to monitor in real time the temperature during the reaction inside the bed. The temperature profile was also recorded by a temperature data logger. The reactions examined in the current study had initial temperatures of 150˚C, 300˚C and 500˚C, whereas the temperature of the oven during the reaction was kept constant at the corresponding temperatures. The reason for choosing this temperature range is to investigate the effect of temperature and the formation of the by-products. According to previous outcomes [37], the possible by-products are expected to be LiOH, $LiOH.H_2O$ and/or Li_2O. The amount of the produced hydrogen was measured by using the volumetric water displacement method as illustrated as the last step in Fig. 1.

3. Results and Discussion

3.1 LiH hydrolysis for initial temperature 150 ^{o}C

The evolution of the LiH hydrolysis when the initial temperature of the material was 150 ^{o}C is presented in Fig. 2, where both the hydrogen production rate (in units of hydrogen production capacity) and the temperature are presented. The maximum amount of hydrogen produced in those conditions was 96% of the theoretical amount of hydrogen. The reaction rate is fast at the first phase of the process (within the first three minutes), where more than

40% of the total hydrogen amount has been produced. Since the hydride powders are very hygroscopic, and they are able to absorb water steam at the beginning of the hydrolysis, the initial hydrogen generation rate is expected to be higher comparing to the upcoming phases of the reaction. At the same time, due to the exothermic nature of the reaction, the temperature of the material increases and reaches a maximum at 196^{o}C after the first 5 min of the reaction.

During the second phase of the reaction, the hydrogen production proceeds, although at that point the production rate is slower and the necessary time to reach a production capacity of 90% is an extra 15 min, as also indicated in Fig. 2. This behaviour is explained by considering the formation of the by-product layers that are eliminating and decelerating the water diffusion towards the unreacted LiH. At that stage, as also the reaction decelerates, the temperature of the material tends to drop, as the exothermic reaction is weaker. The constant temperature of the furnace at 150 ^{o}C also contributes to the temperature decrease of the material due to conduction heat transfer.

At the final phase of the reaction, the hydrogen generation capacity has reached a plateau and the further introduction of steam does not strongly enhance the reaction. During that stage, the temperature of the reacted material tends to reach the initial temperature (150 ^{o}C). There are two major reasons that the material didn't release the total theoretical amount of hydrogen: first, the formation of the by-products didn't allow any more steam to enter the space where the small amount of unreacted LiH is placed. This behaviour is schematically explained in Fig. 2b on a simplified cyclical model. A second explanation might arise from the fact that the hydrolysis reactions might not proceed completely. Hydrolysis is believed to occur either with the formation of the LiOH layer first and then with the formation of Li_2O, or either with the formation of Li_2O first and then the formation of LiOH at the surface. Further discussion regarding the possible reactions will be at *3.6*. The equations are the following:

$LiH(s) + H_2O(g) \rightarrow LiOH(s) + H_2(g)$ (Eq. 1)

$LiOH(s) + LiH(s) \rightarrow Li_2O(s) + H_2(g)$ (Eq. 2)

or

$2LiH(s) + H_2O(g) \rightarrow Li_2O(s) + 2H_2(g)$ (Eq. 3)

$Li_2O(s) + H_2O(g) \rightarrow 2LiOH(s)$ (Eq. 4)

In Eq. 4, it is expected that not all the quantity of Li_2O will react with the steam to form LiOH, as a small amount of Li_2O is necessary to be between the LiH/LiOH, as the coexistence of these two materials is thermodynamic unfavourable. As a result, from this reaction is expected that not all the stoichiometric of LiOH will be produced. The same can be extracted from Eq. 2, where again, maybe not all LiOH will react to produce the oxide and hydrogen.

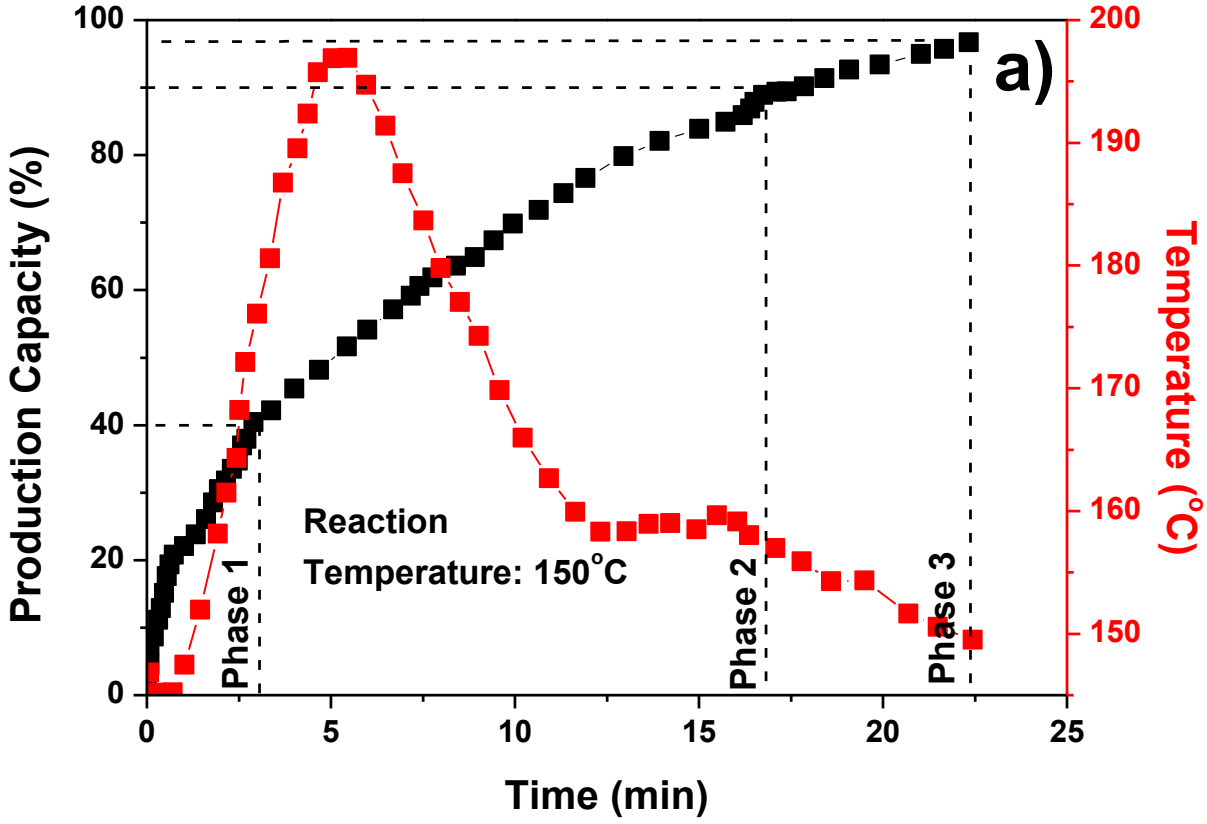

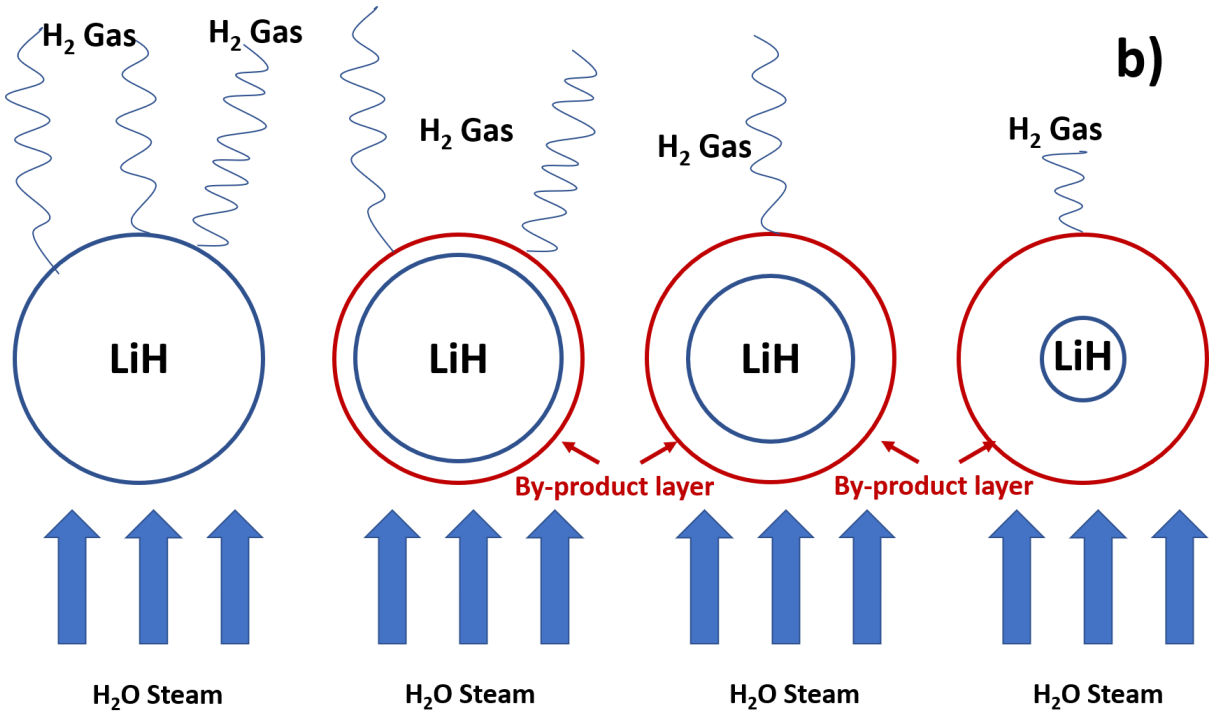

Fig. 2. Hydrogen production capacity and temperature change for LiH hydrolysis at 150 °C, where a final hydrogen production yield of 96% is achieved (2a) and schematic of the effect of the by-product formation on the hydrogen production pace (2b).

3.2 LiH hydrolysis for initial temperature of 300°C

The second case investigates the hydrolysis reaction when the initial temperature of LiH is 300 ^{o}C. The hydrogen production capacity and the temperature evolution during the reaction are presented in Fig. 3. After the first 3 min of the reaction, almost 60% of the total theoretical amount of hydrogen has been produced. The temperature, due to exothermic nature of the reaction itself, increases rapidly and within the first 4 min, a maximum temperature at 625 ^{o}C is observed. At the time that the temperature reaches the maximum value, the production capacity is at the 72% of the maximum amount of hydrogen to be released, as highlighted in Fig. 3. From the shape of the plot for the production capacity, various outcomes are identified; as explained in the previous case, three phases for the hydrolysis reaction are identified. In that case, the first phase is the rapid hydrogen release at the first 30 s of the reaction, where the steam can easily approach and come in contact with the unreacted LiH and initiate the reaction. After that initial stage, LiOH and Li_2O layers are formed, forcing the reaction to slow down. This is represented in Fig. 3, with the curve starting from 0.5 min to almost 5 min. Finally, the last stage of the hydrolysis, where the

reaction reaches a plateau, begins after the fifth minute and the hydrogen produced reaches up to 97% of the maximum theoretical release.

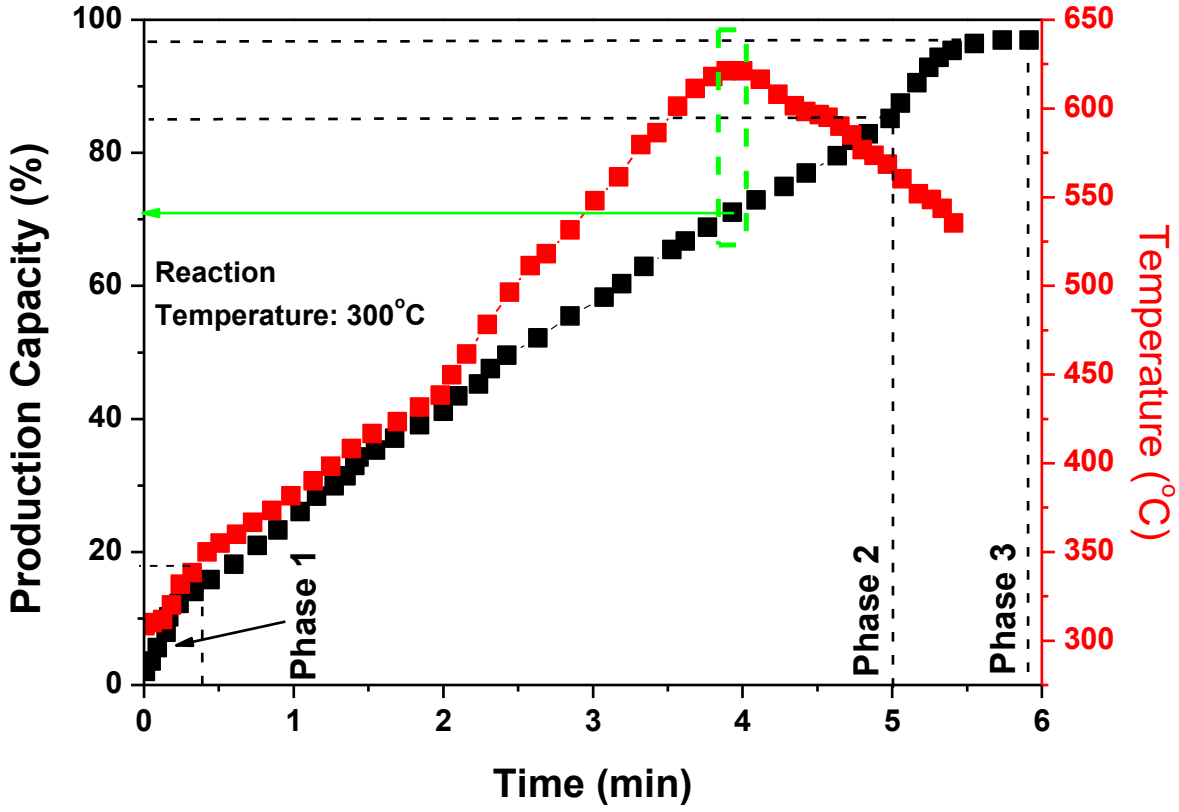

Fig. 3. Hydrogen production capacity and temperature change for LiH hydrolysis at 300 °C, where a maximum hydrogen production yield of 98% is achieved.

3.3 LiH hydrolysis for initial temperature of 500°C

The hydrolysis reaction was also investigated at a higher initial temperature (500 °C). The capacity profile and the temperature evolution are presented in Fig. 4. The hydrogen capacity profile during the reaction is different from the previous cases. At the time where the steam comes in contact with LiH (assumed as t = 0 s), the amount of hydrogen that was recorded was around 15%, indicating that the reaction was rapid by the time the steam was introduced to the system. For that case, the first phase of the reaction is very fast, and it was too fast to be captured on the recordings for the reaction rate. In Fig. 4, this phase is highlighted at the beginning of the reaction. After the first phase of the hydrolysis, the reaction was proceeding at a slower pace, reaching a production of 87% after 7 min of reaction. The temperature up to

that point of the reaction was close to 550 ^{o}C, when suddenly, after the sixth minute of the reaction started to increase rapidly up to almost 700 ^{o}C, where also the production of hydrogen reached the maximum amount (almost 100%).

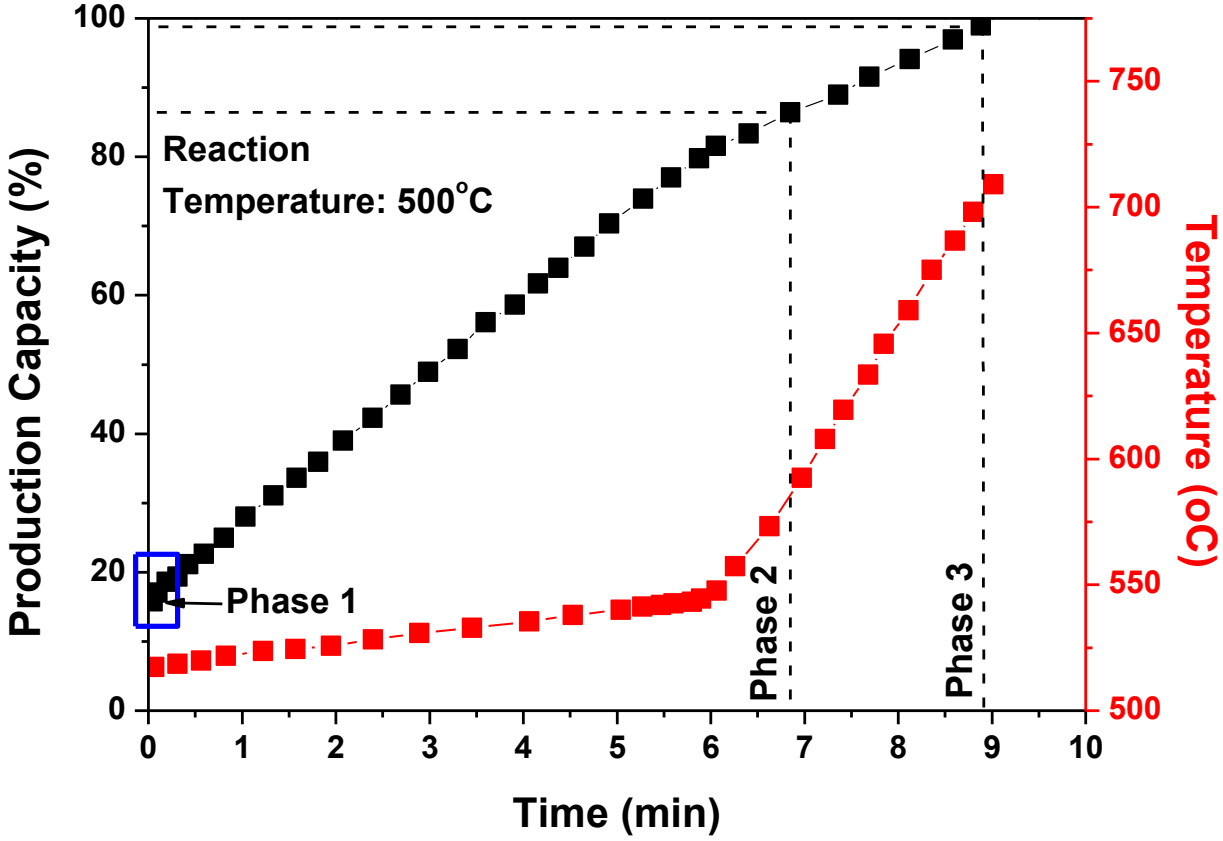

Fig. 4. Hydrogen production capacity and temperature change for LiH hydrolysis at 500 °C, where a maximum hydrogen production yield of almost 100% is achieved.

3.4 Comparison and discussion of the studied cases

For the purposes of the present study, the hydrolysis reaction when steam was introduced in the reactor was examined at three different initial temperatures, 150, 300 and 500 ^{o}C. The comparison for the hydrogen production capacity for all the three cases is presented in Fig. 5. All the studied cases have a common denominator; the reaction can be divided into three phases. The first phase of the hydrolysis begins when the steam comes in contact with the fresh and unreacted LiH surface. For the first moments, the hydrogen production is intense and fast. The first phase doesn't last more than 1-3 min (depending on the reaction

temperature), and for all the cases the hydrogen produced during that period is sufficient. For the clearer and detailed comparison of the first three minutes of the reaction for all the cases, an inlaid picture has been introduced in Fig. 5. It is clear that for all three cases, the production of hydrogen can reach up to 20% of the total amount of hydrogen within the first minute of the reaction; especially for the case of hydrolysis at 500 ^{o}C the hydrogen production is instantaneous and just at the time that the steam is introduced to the reactor the amount of hydrogen produced is almost 15% of the total theoretical amount. By comparing the slopes of the curves for the first minute of the reaction, the hydrolysis rate at 150 and 300 ^{o}C present a similar trend, while the reaction rate at 500^{o}C was slower at the first minute. After the end of the initial hydrogen production, where the fresh surface of LiH comes in direct contact with the steam, the reaction begins to slow down. The reason for that behaviour is the formation of the LiOH and Li_2O layers, as also revealed from the XRD analysis (see 3.5), that play the role of obstacles to the diffusion of water towards the LiH. This behaviour corresponds to the second phase of the reaction. According to Fig. 5, during that phase, the reaction rate when the initial temperature was 300 and 500 ^{o}C has almost the same trend and is faster than the reaction rate for the case of 150 ^{o}C. This behaviour indicates that the layers of LiOH and Li_2O at elevated temperature needs more time to be formed, compared to lower temperatures. The final phase of the reaction appears when almost all hydrogen has been released from the hydride; thus, during the final minutes of the reaction, a plateau appears where the amount of hydrogen released is very small and in general the rate of reaction is very slow. The oxide and hydroxide layers have been developed at that stage and the morphology of the material (remaining LiH and by-products) at the end of the reaction is a white bulk material as shown in Fig. 6. It has to be mentioned that for all the studied initial temperatures, the texture of the final by-product was similar.

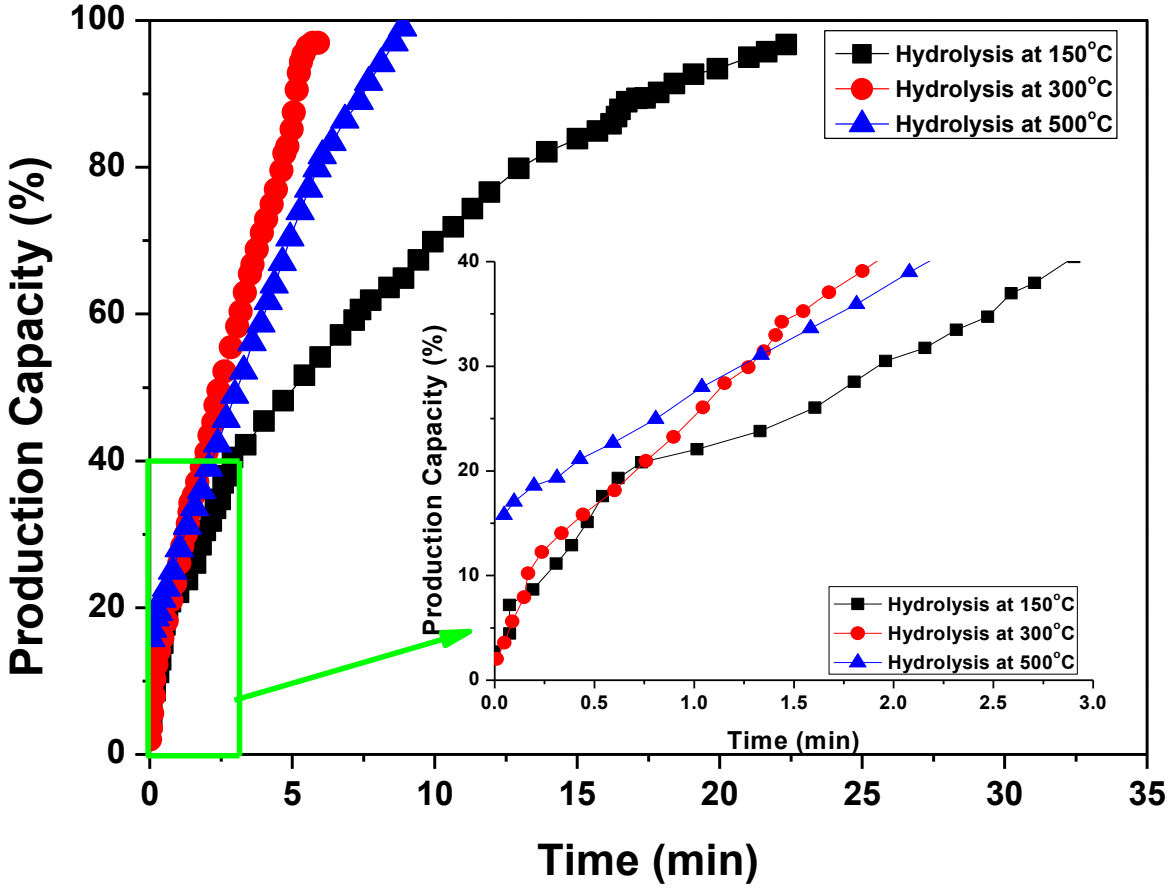

Fig. 5. Production capacity for all the studied cases. On the inlaid the capacity during the first 3 minutes of the reaction is presented.

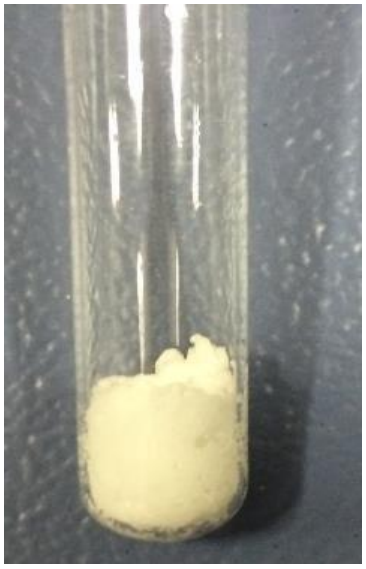

Fig. 6. Image of the by-products at the end of the reaction: a white bulk material was observed in the reaction tube. Similar texture was observed for all the studied cases.

3.5 Characterisation of the reaction by-products

3.5.1 X-ray Diffraction Characterisation of the Reaction By-Products

The X-ray structural characterization of the reaction by-products was performed by utilising a Bruker D8 Advanced Diffractometer. The final material (mostly reaction by-products) was crushed into powder by using a mortar and a pestle in the glove-box. The coupled high-resolution powder X-ray LynxEye position detector and the monochromatic Cu radiation generate the diffraction lines. The powder was scanned and recorded at room temperature in the two theta range from 15° to 70°, with 0.02° step size and CuKα radiation, λ=0.154 nm and K=0.9. The XRD patterns were matched and assigned according to the XRD database provided by International Centre for Diffraction Data (ICDD). Fig. 7 presents the XRD spectrum of the by-product after the hydrolysis reaction at initial temperature of 500 ^{o}C. The phases identified were LiOH (01-076-1073), Li_2O (00-012.0254) and small amount of $LiOH{\cdot}H_2O$ (00-032-0564). The main peaks for LiOH were identified at the following angles: 20.39^{o} – 32.63^{o} – 35.87^{o} and 49.04^{o}. For the Li_2O phase, the main peaks were identified at: 33.57^{o} – 64.22^{o} and 65.33^{o}. In addition, a comparison of the XRD spectra for the hydrolysis reactions taken place at initial temperature of 150 ^{o}C (low temperature) and 500^{o}C (high

temperature) is presented in Fig. 8. For the lower temperature reaction, two extra peaks at 21.5^{o} and 43.2^{o} are present, corresponding to LiOH•H_2O phase. The reason for that behaviour is explained in paragrapg 3.6, where the Gibbs free energy analysis of all the reactions is introduced.

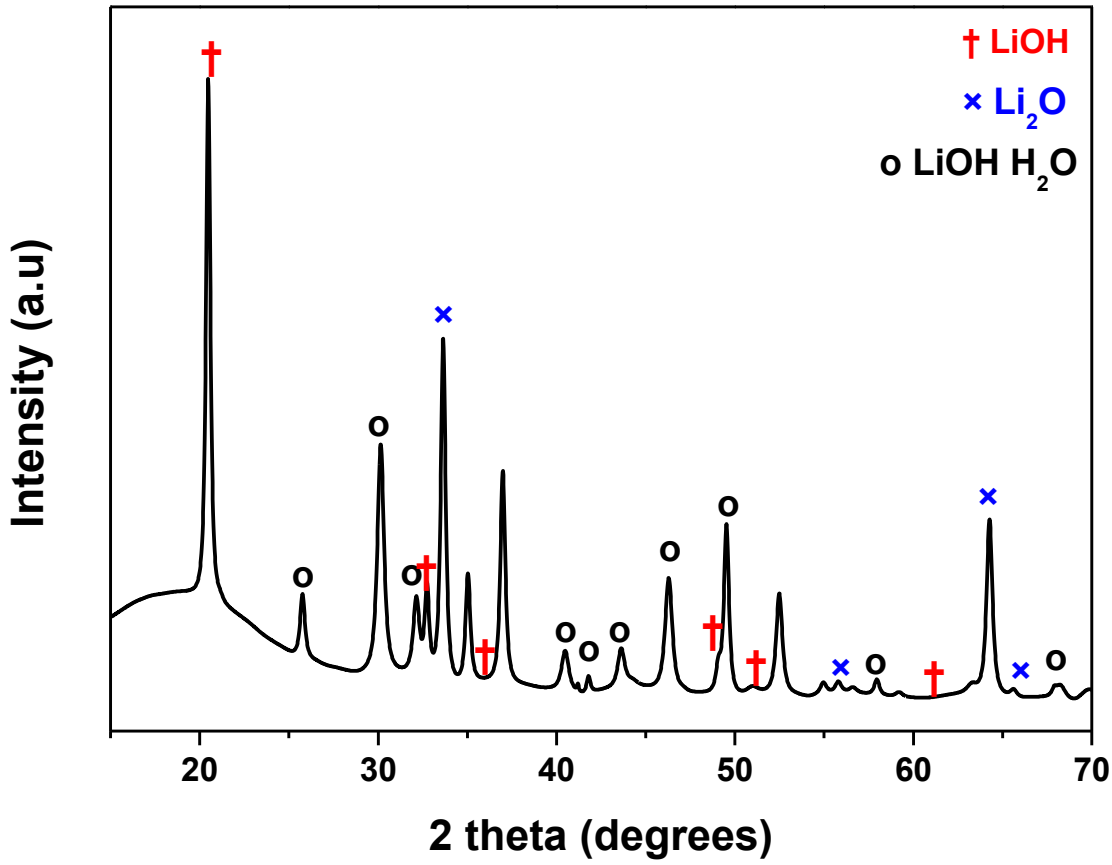

Fig. 7. X-ray diffraction patterns for the by-products of the reaction at 500 ^{o}C

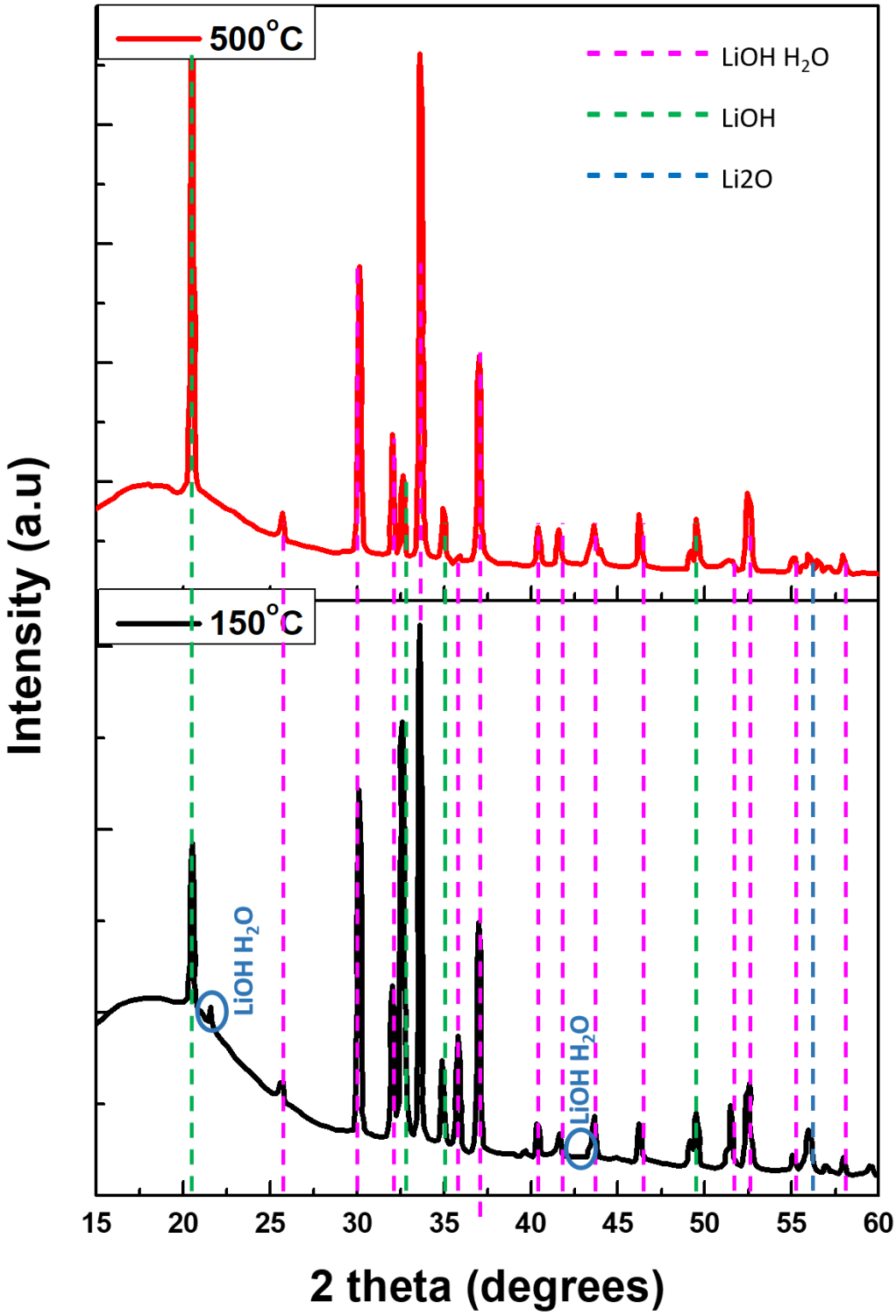

Fig. 8. Comparison of the X-ray diffraction patterns of the by-products for the reaction taken place at 150 °C (down spectra) and at 500 °C (upper spectra)

3.6 Gibbs Free Energy and Chemical Equilibrium Analysis

Table 1 summarises all the possible reactions that can occur at various temperatures up to 800 ^{o}C. From the listed 6 equations, the calculation on the change of the Gibbs free energy (ΔG^{o}) has been utilised for each one, under a wide range of reaction temperatures. More specifically, out of the thermodynamic point of view, the Gibbs free energy is the thermodynamic potential that receives the minimum value when a system reaches chemical equilibrium under constant temperature and pressure.

The importance for calculating these values is that a direct indication of the reaction balance between the two driving forces for the reaction (enthalpy and entropy) can be extracted and it determines whether the reaction is spontaneous or not. When the ΔG receives a negative value, the reaction should be favorable or spontaneous, while the opposite effect should take place when ΔG receives a positive value. The ΔG can be calculated from the equation below:

$$\Delta G = \Delta H - T\Delta S,$$

where ΔG is the change of the Gibbs free energy (kJ), ΔH is the change in enthalpy (kJ), ΔS is the change in entropy (kJ/K) and T is the reaction temperature (K).

Table 1: List of the possible hydrolysis reactions.

Reaction	Enthalpy Change	
$LiH_{(s)} + H_2O_{(g)} \rightarrow LiOH_{(s)} + H_{2(g)}$	$\Delta H^{\circ}_{298.15} = -152.5\ kJ/mol$	Eq.1
$LiH_{(s)} + 2H_2O_{(g)} \rightarrow LiOH.H_2O_{(s)} + H_{2(g)}$	$\Delta H^{\circ}_{298.15} = -216.1\ kJ/mol$	Eq.2
$LiOH_{(s)} + H_2O_{(g)} \rightarrow LiOH.H_2O_{(s)}$	$\Delta H^{\circ}_{298.15} = -63.6\ kJ/mol$	Eq.3
$\mathrm{LiH_{(s)}} + \frac{1}{2}\mathrm{H_2O_{(g)}} \rightarrow \frac{1}{2}\mathrm{Li_2O_{(s)}} + \mathrm{H_{2(g)}}$	$\Delta H^{\circ}_{298.15} = -87.8\ kJ/mol$	Eq.4
$\mathrm{LiH_{(s)}} + LiOH_{(s)} \rightarrow \mathrm{Li_2O_{(s)}} + \mathrm{H_{2(g)}}$	$\Delta H^{\circ}_{298.15} = -23.2\ kJ/mol$	Eq.5
$Li_2O(\mathrm{s}) + \mathrm{H_2O_{(g)}} \rightarrow 2LiOH$	$\Delta H^{o}_{298.15} = -129.3 kJ/mol$	Eq.6

Fig. 9 presents the ΔG values as calculated for all the possible hydrolysis reactions over a wide temperature range (from 25 ^{o}C to 800 ^{o}C with an increase step of 25 ^{o}C). The Gibbs free energy analysis of the reactions showed that at the temperature of 150 °C, the dominant reactions are those described by Eq. 1 (Reaction 1) and Eq. 2 (Reaction 2). The outcome of this analysis is that the main by-products at that temperature are expected to be LiOH and LiOH•H_2O, but also some oxides as secondary by-products, described by Eq. 4 (Reaction 4) might be present. For the temperature 300 ^{o}C, the dominant reaction is the one described by Eq. 1 (Reaction 1), indicating that the main by-product should be LiOH, while at that

temperature also the reactions described by Eq. 2 and Eq. 4 are feasible, indicating the presence of Li_2O and $LiOH.H_2O$. Furthermore, the reaction described in Eq. 5 (Reaction 5), as the temperature increases becomes more spontaneous, will lead to a higher amount of Li_2O as by-product. Considering the higher temperature that has been studied (500 ^oC), both the reactions described by Eq. 1 (Reaction 1) and Eq. 4 (Reaction 4) are playing key role, indicating that the main by-products in that case should be LiOH and Li_2O. The results from the Gibbs free energy analysis are also supported from the comparison of the XRD spectra presented in Fig. 8. The presence of a larger amount of $LiOH•H_2O$ as by product for the low temperature reaction (150 ^oC) indicates that the reactions 2 and 3 are dominant at that temperature, whereas the presence of Li_2O in the by-products of the reaction initiated at 500 ^oC is indicated in Fig. 7.

The analysis and the calculation of ΔG to extract information regarding the by-product formation indicated the temperature at which each reaction is possible to occur. As the temperature increases, lighter by-products are formed. This behaviour shows the potential for larger amounts of hydrogen to be produced, as extracted from the Eq. 1, Eq. 2, Eq. 4 and Eq. 5. Therefore, the by-product can form a protecting layer that prevents the steam access and reduce the capability of the steam to diffuse towards the unreacted layers of LiH.

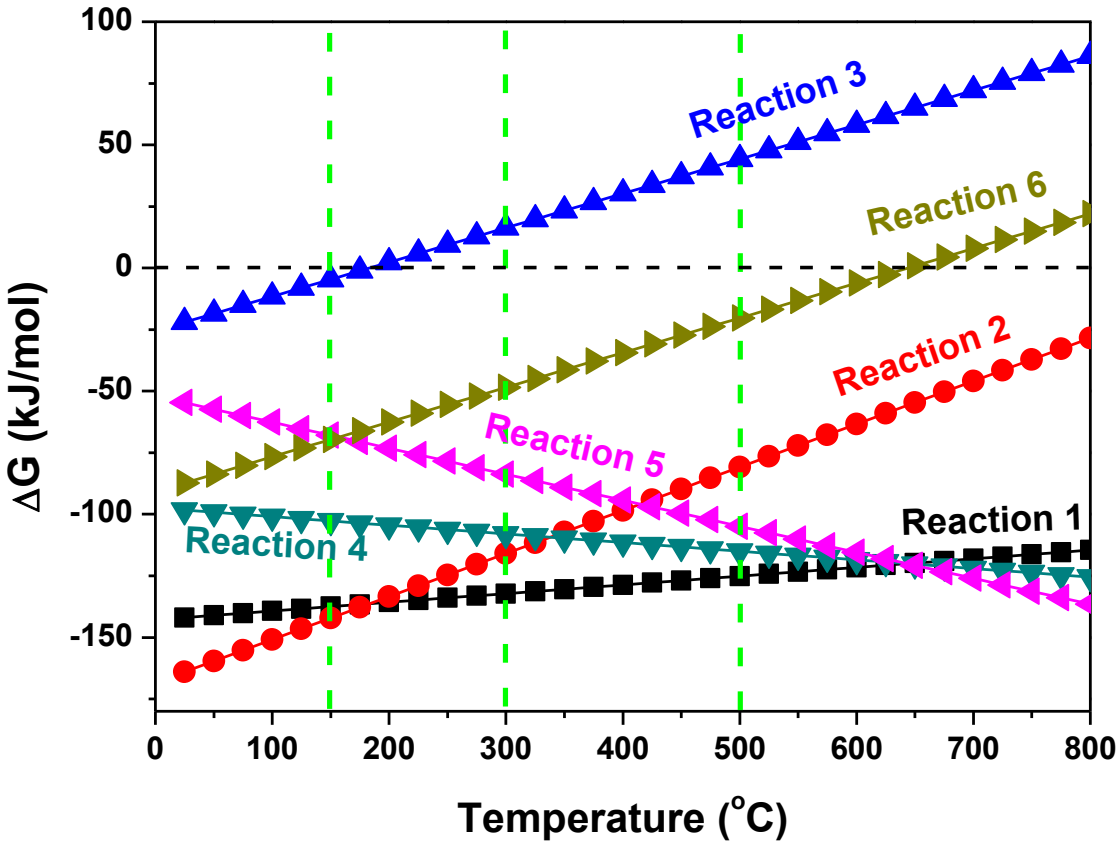

Figure 9. Gibbs free energy calculations for possible lithium hydride hydrolysis up to 800 °C.

For this reason, a chemical equilibrium analysis regarding the LiH hydrolysis reaction was considered by utilising the Chemical Equilibrium with Applications (CEA) software provided by NASA [48]. This software calculates the chemical equilibrium compositions of complex mixtures. In the case of the LiH hydrolysis, the chemical equilibrium product concentrations from any set of LiH hydrolysis reactants are considered and the software provides the thermodynamic and transport properties for the product mixture. The results extracted from the software are presented in Fig. 10. According to the results, it can be further confirmed that the reaction by-products are H_2 and LiOH for temperature ranges up to 400 °C; then for the reaction at higher temperatures the products are H_2, Li_2O and unreacted water.

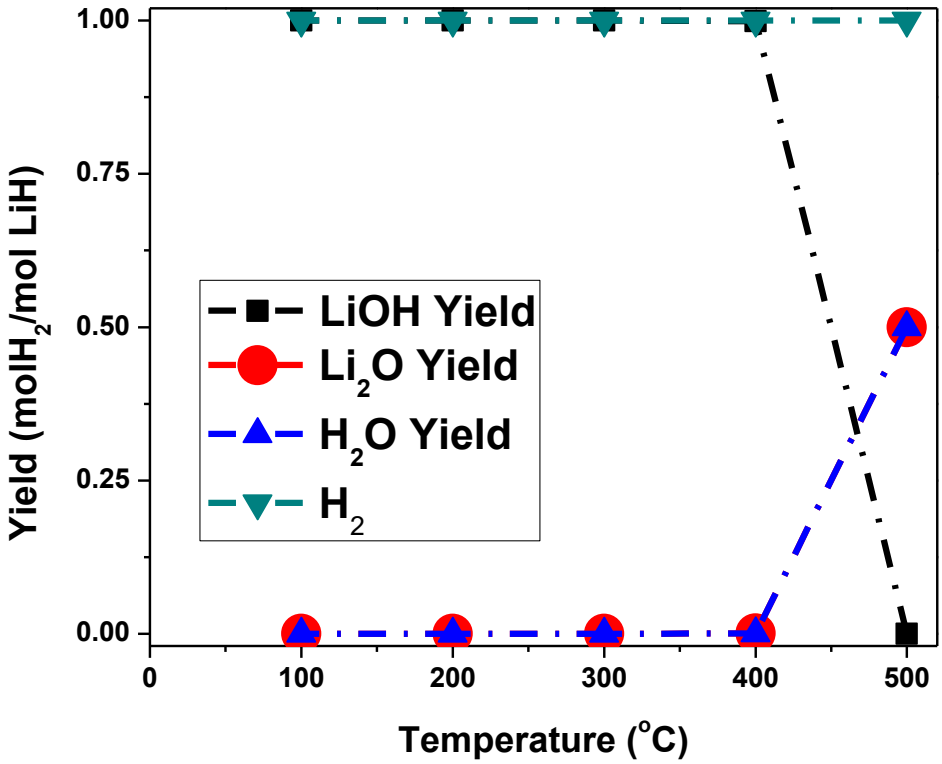

Fig. 10. Chemical Equilibrium Analysis (CEA) for LiH hydrolysis and expected products yield.

3.7 Implementation of the Hydrogen Production System to a UAV Prototype

One of the main challenges for the implementation and commercialisation of hybrid electric/fuel cell and/or purely fuel cell UAVs is the on-board hydrogen production and storage, as well as safety during the operation. The main target of the current work was the identification of the possibility to utilise the hydrogen that is produced from the hydrolysis of LiH to feed a fuel cell for a hybrid electric or a purely fuel cell-based UAV. The main idea is the usage of the LiH tank as main or as secondary (backup) hydrogen source. The produced hydrogen can be used either for feeding the fuel cell during the flight and smooth the peak power applied to the battery for hybrid electric/FC UAVs to elongate the flight time or even for urgent situations, such as emergency landing. From the analysis of the hydrogen production characteristics presented in the previous sections, it can be extracted that the usage of LiH as hydrogen source has the potential to be applied to the aviation sector, as the hydrogen is produced on a fast pace and, in addition, almost all the stoichiometric amount of hydrogen can be extracted from LiH when steam is supplied to the material. Besides the

benefits that LiH offers as a medium for hydrogen production, it must be handled carefully during the operation in order to avoid any contact with the atmosphere. For that reason, effective tanks have to be designed. The tanks should be made from a light material to reduce as much as possible the extra weight in the UAV frame. A possible design for the hydrogen production tanks is presented in Fig. 11. The tank is of cylindrical shape and two end caps will be applied. The first end cap (the right in Fig. 11) will be fixed to the reactor, while the second one will be movable, in order to be able to clean and refill the reactor after the operation. The LiH powder will be placed in the centre of the reactor and a movable double mesh will be placed vertical to the cylinder to prevent the possibility that LiH powder will come out of the system; thus, only steam will enter the reactor. Depending on the UAV and the specifications regarding the flight time and the payload capacity, the amount of LiH and consequently the number of reactors that will be equipped in the UAV will vary.

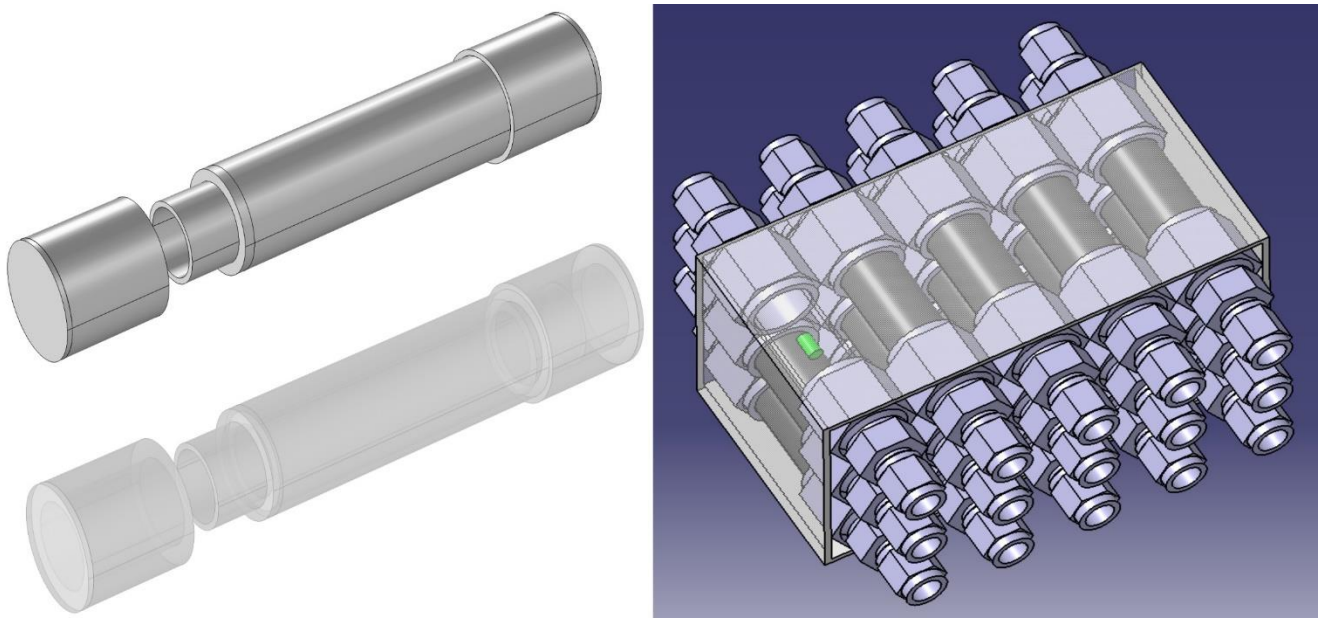

Fig. 11. Schematic of the hydrogen production reactors to be implemented in the UAV frame

Another challenge for the implementation of the fuel cell – hydrogen production system and the high-pressure hydrogen cylinder is the identification of an effective power undercarriage mechanical design that will be able to incorporate all the parts. The reference drone that has been used for the analysis is a D800-X8 octocopter as depicted in Fig. 12b and 12c. [49], with a frame weight of 3.7 kg and take-off weight of 4-10 kg. The flight time for the current drone is up to 18 min when the battery nominal power is 20,000 mAh and the total weight is 6.7 kg.

The key objective was to modify the frame of the current UAV and develop a propulsion system that will be based on the combination between batteries (for the case of the hybrid system), the fuel cell, the hydrogen production unit and the high-pressure hydrogen cylinder. The main idea is presented in Fig. 11a. The batteries will be installed on the top of the frame as indicated in Fig. 12a, while the hydrogen system will be installed underneath the main body of the drone (12a). For the hydrogen system an extra frame/platform has been introduced as seen in Fig. 12d. The platform for the payload is suspended from a ball and socket joint thus allowing to sway with a small degree of rotation. Having the platform hanging independent of the crash frame also means that during a collision, the collision energy does not directly affect the payload until the hanger comes into contact with the hanging plate. To balance the payload on the hanger, the most substantial component, the fuel cell was placed in the centre, whereas the hydrogen tank and the hydrogen production system were selected to be on each side of the fuel cell, as also depicted in Fig. 12d and 12e. In addition, to add extra protection to the hydrogen system, side panels were introduced to the original frame of the drone, as it can be seen in Fig. 12f. For the case of an uncontrolled landing, in order to enhance the possibilities to protect the system, an idea of installing an airbag was introduced (Fig. 12f and 12g). The airbag system will be situated in the space between the bottom platform of the hanger and the crash undercarriage. With the tank placed on the opposite side of the platform from the hydrogen tank as to mass balance the system. The inflation tube will slot through the plate (Fig. 12g). The platform also acts to force the inflating airbag downward and away from the vital components. It is intended that the airbag inflation mechanism used will be one of similar to those commercially available for cycle safety but over a larger area. The airbag has been designed to be rectangular, with the hemispherical ribs to increase the surface area. When inflating due to impact, the bottom plate would have already been damaged so the bag will inflate at maximum velocity to protect the fuel cell and tanks in the same way a conventional airbag inflates.

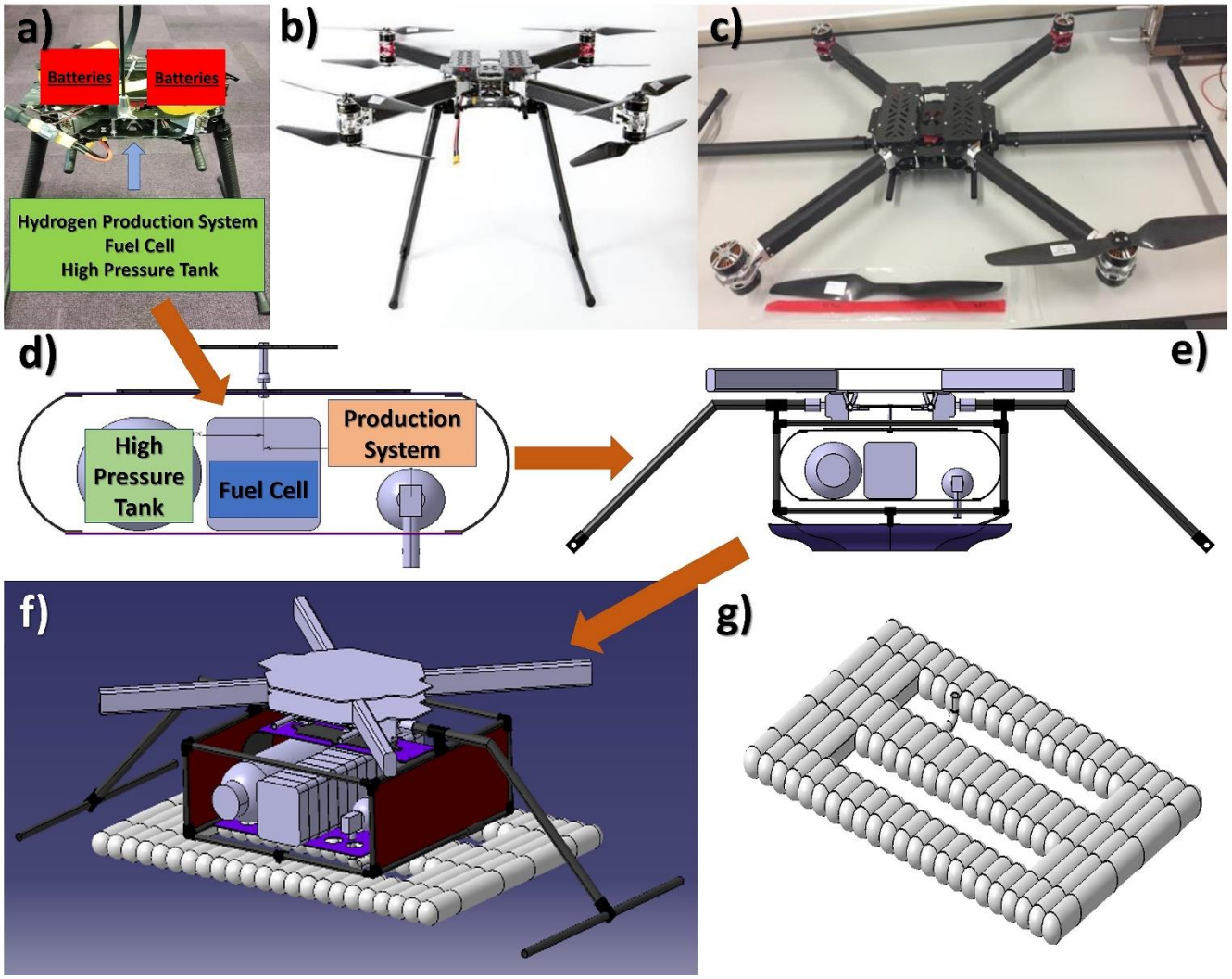

Fig. 12. Schematic of the design to implement and protect the hydrogen system. Fig. 11a shows the positions that the batteries and the hydrogen system will be places, while Fig. 11b and 11c present the UAV actual and original frame. The case of implementing the hydrogen system is presented in Fig. 11d and 11e, while the protection of the hydrogen system is described in Fig. 11f and 11g.

4. Conclusion

In the present work, the LiH hydrolysis reaction was studied, to identify the possibility of using an on-board hydrogen production system for fuel cell-based UAVs. The hydrolysis reaction was studied at various oven temperatures/initial temperatures of the powders (150 ^{o}C, 300 ^{o}C and 500 ^{o}C). The by-products of the reaction were also studied to identify the by-product layer formation and their role to the hydrogen production capacity as well as the rate

of reaction. For all the temperatures, the hydrogen production reached almost the maximum possible value, but on the other hand, the reaction pace was different at each case. This behaviour indicates that although the formation of the by-product layers does not affect the hydrogen release capability, it affects the reaction kinetics. To get a clearer indication of the by-product formation, X-ray diffraction analysis considered, where at the same time the Gibbs free energy and the chemical equilibrium analysis applied to recognize the thermodynamic potential for the by-product formation. Finally, the initial concept regarding the addition of an on-board hydrogen production system in fuel cell-based UAVs was also investigated. For that scenario, an effective power undercarriage mechanical design that will be able to incorporate the battery (for the case of hybrid electric/FC UAV), the fuel cell, the storage tank and the hydrogen production system was introduced. The analysis of the reaction kinetics and the by-products will be useful for future development of liquid water - LiH hydrogen hydrolysis generator that will be sufficient to produce hydrogen at low operation temperature.

Acknowledgement

The authors wish to acknowledge the Coventry University ECR Schemes that supported financially the project

References

[1] Dincer I, Acar C. Innovation in hydrogen production. Int J Hydrogen Energy 2017;42:14843–64. doi:https://doi.org/10.1016/j.ijhydene.2017.04.107.

[2] Gkanas EI, Steriotis TA, Stubos AK, Myler P, Makridis SS. A complete transport validated model on a zeolite membrane for carbon dioxide permeance and capture. Appl Therm Eng 2015;74. doi:10.1016/j.applthermaleng.2014.02.006.

[3] Khzouz M, Gkanas EI, Du S, Wood J. Catalytic performance of Ni-Cu/Al2O3 for effective syngas production by methanol steam reforming. Fuel 2018;232:672–83. doi:https://doi.org/10.1016/j.fuel.2018.06.025.

[4] Abdalla AM, Hossain S, Nisfindy OB, Azad AT, Dawood M, Azad AK. Hydrogen production, storage, transportation and key challenges with applications: A review. Energy Convers Manag 2018;165:602–27. doi:https://doi.org/10.1016/j.enconman.2018.03.088.

[5] Gkanas EI. 5 - Metal hydrides: Modeling of metal hydrides to be operated in a fuel cell. In: Ferreira-Aparicio P, Chaparro AM, editors. Portable Hydrog. Energy Syst., Academic Press; 2018, p. 67–90. doi:https://doi.org/10.1016/B978-0-12-813128-2.00005-X.

[6] Gondal IA, Masood SA, Khan R. Green hydrogen production potential for developing a hydrogen economy in Pakistan. Int J Hydrogen Energy 2018;43:6011–39. doi:https://doi.org/10.1016/j.ijhydene.2018.01.113.

[7] Makridis SS, Gkanas EI, Panagakos G, Kikkinides ES, Stubos AK, Wagener P, et al. Polymer-stable magnesium nanocomposites prepared by laser ablation for efficient hydrogen storage. Int J Hydrogen Energy 2013;38. doi:10.1016/j.ijhydene.2013.04.031.

[8] Stehlík K, Tkáč M, Bouzek K. Recent advances in hydrogen technologies in the Czech Republic. Int J Hydrogen Energy 2018. doi:https://doi.org/10.1016/j.ijhydene.2018.07.191.

[9] Chen Y-T, Hsu C-W. The key factors affecting the strategy planning of Taiwan's hydrogen economy. Int J Hydrogen Energy 2018. doi:https://doi.org/10.1016/j.ijhydene.2018.07.159.

[10] Dincer I, Acar C. Smart energy solutions with hydrogen options. Int J Hydrogen Energy 2018; 43:8579–99. doi:https://doi.org/10.1016/j.ijhydene.2018.03.120.

[11] Brilliantova V, Thurner TW. Blockchain and the future of energy. Technol Soc 2018. doi:https://doi.org/10.1016/j.techsoc.2018.11.001.

[12] Mohan A, Topp K. India's energy future: Contested narratives of change. Energy Res Soc Sci 2018;44:75–82. doi:https://doi.org/10.1016/j.erss.2018.04.040.

[13] Gkanas EI, Statheros T, Khzouz M. Heat management on rectangular metal hydride tanks for green building applications. Int J Hydrogen Energy 2018. doi:https://doi.org/10.1016/j.ijhydene.2018.06.030.

[14] Chen S, Kumar A, Wong WC, Chiu M-S, Wang X. Hydrogen value chain and fuel cells within hybrid renewable energy systems: Advanced operation and control strategies. Appl Energy 2019;233–234:321–37. doi:https://doi.org/10.1016/j.apenergy.2018.10.003.

[15] Gkanas EI, Khzouz M, Panagakos G, Statheros T, Mihalakakou G, Siasos GI, et al. Hydrogenation behavior in rectangular metal hydride tanks under effective heat management processes for green building applications. Energy 2018;142. doi:10.1016/j.energy.2017.10.040.

[16] de Miguel C, Filippini M, Labandeira X, Löschel A. Informing the Transitions towards Low-carbon Societies. Energy Econ 2017;68:1–3. doi:https://doi.org/10.1016/j.eneco.2018.01.031.

[17] Stygar M, Brylewski T. Towards a hydrogen economy in Poland. Int J Hydrogen Energy 2013;38:1–9. doi:https://doi.org/10.1016/j.ijhydene.2012.10.056.

[18] E.I. Gkanas, M. Khzouz, Metal Hydride Hydrogen Compression Systems–Materials, Applications and Numerical Analysis, Hydrogen Storage Technologies. Sankir, M. & Sankir, N. D. (eds.). 1 ed. USA: Wiley, Vol. 1, p. 3-37 35

[19] Touili S, Merrouni AA, Azouzoute A, Hassouani Y El, Amrani A. A technical and economical assessment of hydrogen production potential from solar energy in Morocco. Int J Hydrogen Energy 2018;43:22777–96. doi:https://doi.org/10.1016/j.ijhydene.2018.10.136.

[20] Mohsin M, Rasheed AK, Saidur R. Economic viability and production capacity of wind generated renewable hydrogen. Int J Hydrogen Energy 2018;43:2621–30. doi:https://doi.org/10.1016/j.ijhydene.2017.12.113.

[21] ezzahra Chakik F, Kaddami M, Mikou M. Effect of operating parameters on hydrogen production by electrolysis of water. Int J Hydrogen Energy 2017;42:25550–7. doi:https://doi.org/10.1016/j.ijhydene.2017.07.015.

[22] Khzouz M, Gkanas E. Experimental and Numerical Study of Low Temperature Methane Steam Reforming for Hydrogen Production. Catalysts 2017. doi:10.3390/catal8010005.

[23] Tian T, Li Q, He R, Tan Z, Zhang Y. Effects of biochemical composition on hydrogen production by biomass gasification. Int J Hydrogen Energy 2017;42:19723–32. doi:https://doi.org/10.1016/j.ijhydene.2017.06.174.

[24] Kovač A, Marciuš D, Budin L. Solar hydrogen production via alkaline water electrolysis. Int J Hydrogen Energy 2018. doi:https://doi.org/10.1016/j.ijhydene.2018.11.007.

[25] Awbery RP, Tsang SC. Novel determination of surface temperature of lithium hydride hydrolysis using DRIFT spectroscopy. J Nucl Mater 2008;381:223–30. doi:https://doi.org/10.1016/j.jnucmat.2008.07.010.

[26] Liu Y, Wang X, Liu H, Dong Z, Cao G, Yan M. Hydrogen generation from Mg–LiBH4 hydrolysis improved by AlCl3 addition. Energy 2014;68:548–54. doi:https://doi.org/10.1016/j.energy.2014.01.005.

[27] Maupoix C, Houzelot JL, Sciora E, Gaillard G, Charton S, Saviot L, et al. Experimental investigation of the grain size dependence of the hydrolysis of LiH powder. Powder Technol 2011;208:318–23. doi:https://doi.org/10.1016/j.powtec.2010.08.023.

[28] Chen W, Ouyang LZ, Liu JW, Yao XD, Wang H, Liu ZW, et al. Hydrolysis and regeneration of sodium borohydride (NaBH4) – A combination of hydrogen production and storage. J Power Sources 2017;359:400–7. doi:https://doi.org/10.1016/j.jpowsour.2017.05.075.

[29] Li C, Peng P, Zhou DW, Wan L. Research progress in LiBH4 for hydrogen storage: A review. Int J Hydrogen Energy 2011;36:14512–26. doi:https://doi.org/10.1016/j.ijhydene.2011.08.030.

[30] Gil-San-Millan R, Grau-Atienza A, Johnson DT, Rico-Francés S, Serrano E, Linares N, et al. Improving hydrogen production from the hydrolysis of ammonia borane by using multifunctional catalysts. Int J Hydrogen Energy 2018;43:17100–11. doi:https://doi.org/10.1016/j.ijhydene.2018.06.137.

[31] Kong VCY, Foulkes FR, Kirk DW, Hinatsu JT. Development of hydrogen storage for fuel cellgenerators. i: Hydrogen generation using hydrolysishydrides. Int J Hydrogen Energy 1999;24:665–75. doi:https://doi.org/10.1016/S0360-3199(98)00113-X.

[32] Belmonte N, Staulo S, Fiorot S, Luetto C, Rizzi P, Baricco M. Fuel cell powered octocopter for inspection of mobile cranes: Design, cost analysis and environmental impacts. Appl Energy 2018;215:556–65. doi:https://doi.org/10.1016/j.apenergy.2018.02.072.

[33] Hassanalian M, Abdelkefi A. Classifications, applications, and design challenges of drones: A review. Prog Aerosp Sci 2017;91:99–131. doi:https://doi.org/10.1016/j.paerosci.2017.04.003.

[34] Wang X, Deng Y, Duan H. Edge-based target detection for unmanned aerial vehicles using competitive Bird Swarm Algorithm. Aerosp Sci Technol 2018;78:708–20. doi:https://doi.org/10.1016/j.ast.2018.04.047.

[35] Donateo T, Ficarella A, Spedicato L, Arista A, Ferraro M. A new approach to calculating endurance in electric flight and comparing fuel cells and batteries. Appl Energy 2017;187:807–19. doi:https://doi.org/10.1016/j.apenergy.2016.11.100.

[36] Renau J, Barroso J, Lozano A, Nueno A, Sánchez F, Martín J, et al. Design and manufacture of a high-temperature PEMFC and its cooling system to power a lightweight UAV for a high altitude mission. Int J Hydrogen Energy 2016;41:19702–12. doi:https://doi.org/10.1016/j.ijhydene.2015.12.209.

[37] Haertling C, Hanrahan RJ, Smith R. A literature review of reactions and kinetics of lithium hydride hydrolysis. J Nucl Mater 2006;349:195–233. doi:https://doi.org/10.1016/j.jnucmat.2005.10.005.

[38] Wang L, Quadir MZ, Aguey-Zinsou K-F. Direct and reversible hydrogen storage of lithium hydride (LiH) nanoconfined in high surface area graphite. Int J Hydrogen Energy 2016;41:18088–94. doi:https://doi.org/10.1016/j.ijhydene.2016.07.073.

[39] Guichard J, Bouyer F, Sciora E, Bernard F, Lecoq H, Besnard R, et al. Hydrolysis of lithium hydride under low relative humidity. Int J Hydrogen Energy 2015;40:12736–44. doi:https://doi.org/10.1016/j.ijhydene.2015.07.047.

[40] Gkanas EI, Makridis SS. Effective thermal management of a cylindrical MgH2 tank including thermal coupling with an operating SOFC and the usage of extended surfaces during the dehydrogenation process. Int J Hydrogen Energy 2016;41:5693–708. doi:https://doi.org/10.1016/j.ijhydene.2016.01.165.

[41] Garlea E, King MO, Galloway EC, Boyd TL, Smyrl NR, Bilheux HZ, et al. Identification of lithium hydride and its hydrolysis products with neutron imaging. J Nucl Mater 2017;485:147–53. doi:https://doi.org/10.1016/j.jnucmat.2016.12.012.

[42] Kawakami M, Kuriiwa T, Kamegawa A, Takamura H, Okada M, Kaburagi T. Optimum Hydrogen Desorption Properties in LiH-LiOH Composites. Mater Trans 2009. doi:10.2320/matertrans.M2009055.

[43] Prosini PP, Cento C, Gislon P. Steam Hydrolysis of Lithium Hydride. Int J Green Energy 2010;7:103–15. doi:10.1080/15435070903501316.

[44] Sifuentes A, Stowe AC, Smyrl N. Determination of the role of Li2O on the corrosion of lithium hydride. J Alloys Compd 2013;580:S271–3. doi:https://doi.org/10.1016/j.jallcom.2013.02.046.

[45] Gislon P, Prosini P.P, Devices for producing hydrogen via NaBH4 and LiH hydrolysis. Int J Hydrogen Energy 2011;36:240–6.

[46] Xiao S, Shuai M.B, Chu M.F, Effects of Li2O Thickness and Moisture Content on LiH Hydrolysis Kinetics in Slightly Humidified Argon Int J Chem Mol Nucl Mater Metall Eng 2011; 1063-1067. doi.org/10.5281/zenodo.1059859

[47] Kong VCY, Kirk DW, Foulkes FR, Hinatsu JT. Development of hydrogen storage for fuel cell generators II: utilization of calcium hydride and lithium hydride. Int J Hydrogen Energy 2003;28:205–14. doi:https://doi.org/10.1016/S0360-3199(02)00039-3.

[48] https://www.grc.nasa.gov/www/CEAWeb (last accessed 20/12/2018)

[49] http://www.dys.hk/product/D800-X8.html (last accessed 20/12/2018)